A highly active bimetallic oxides catalyst supported on Al-containing MCM-41 for Fenton oxidation of phenol solution

Min Xia, Mingce Long*, Yudong Yang, Chen Chen, Weimin Cai**, Baoxue Zhou

School of Environmental Science and Engineering, Shanghai Jiao Tong University, Dongchuan Road 800, Shanghai 200240, China
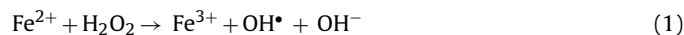
ABSTRACT

A new heterogeneous Fenton catalyst, Fe-Cu bimetallic oxides supported aluminum-containing MCM-41, was synthesized by co-precipitation method. The physicochemical characteristics of the synthesized samples were evaluated by various techniques such as XRD, TEM, nitrogen physisorption, zeta potential and XPS. The incorporation of metal species did not alter the well-ordered hexagonal mesostructure of MCM-41 support. Compared with the monometallic or the Al absent catalysts, this new bimetallic oxides supported aluminum-containing MCM-41 catalyst exhibited a higher activity and stability in phenol mineralization. The effects of temperature, pH and H_2O_2 dosage were investigated in terms of the TOC conversion. At pH 4, 60 °C and 0.049 mol/L of H_2O_2 dosage, a 47% TOC reduction has been achieved. With incorporating aluminum, the increase in surface oxygen-containing groups was observed by zeta potential analysis, the downshift binding energy of active metals was found by XPS measurement, and an enhancement of H_2O_2 utilization ratio was achieved. On the basis of our findings, the beneficial role of Al has been explained.

© 2011 Elsevier B.V. All rights reserved.

1. Introduction

Advanced oxidation technologies (AOT) refer to a set of chemical oxidation procedures designed for wastewater treatment. The AOT procedures have been accepted as an efficient way to remove non-biodegradable toxic organic substances such as aromatics, pesticides, petroleum constituents, and volatile organic compounds in wastewater [1]. Among them, Fenton chemistry is a focused area due to its benign process and general applicability [2,3] in environment remediation. The classical Fenton reagent, consisting of the reaction of homogeneous Fe^{2+}/Fe^{3+} catalysts with hydrogen peroxide (H_2O_2), as shown in Eq. (1), is highly efficient. However, it requires a strong acid condition (pH < 3) to avoid ferrous and ferric ion hydrolysis as well as to achieve acceptable conversion rates. Additionally, non-recyclable soluble iron salts will yield large amounts of iron oxide sludge which need further removal from the treated water. Such drawbacks mentioned above limit the applicability of Fenton chemistry as a general solution for pollution remediation and triggered a great effort to reform it. The heterogeneous catalysts using solid matrixes such as Nafion membranes [4], bentonite [5,6] and zeolites [7–10] for immobilizing iron can be effective alternatives. These heterogeneous Fenton systems have been demonstrated to be useful to treat various organic pollutants in the aqueous environment. However, the heterogeneous Fenton catalyst was relatively slow and awkward if it was operated at high pH values or did not collaborate with external power supplies such as UV [11,12], ultrasound [13] or microwave [14]. These external supplies require extra cost and energy input, which blocked the practical application of Fenton catalysis in wastewater treatment. Thus, it is necessary to improve the activity of heterogeneous catalyst itself to attain the lower fixed capital cost and less power consumption.

$$Fe^{2+} + H_2O_2 \rightarrow Fe^{3+} + OH^\bullet + OH^- \quad (1)$$

$$Cu^+ + H_2O_2 \rightarrow Cu^{2+} + OH^\bullet + OH^- \quad (2)$$

Recently, another metal, copper, which behaves like a Fenton reagent, has attracted great attention. Copper species, as illustrated in Eq. (2) [15], are less pH dependent, so that they can maintain activity in a wide pH range. Such characteristic facilitates the usage of copper catalysts in the industry application. Incorporating copper into an iron containing solid matrix to fabricate a bimetallic oxide catalyst has become a hotspot in the field of Fenton chemistry [16–19]. The resulting materials possessed an improved catalytic activity due to the synergistic effects of two-metal redox couples. On the other side, the effect of aluminum on Fenton catalysis has attracted increasing attention. Lim et al. [20] impregnated iron oxide nanoparticles in alumina coated mesoporous SBA-15 silica to obtain a highly active heterogeneous catalyst. Pham et al. [21] introduced alumina into an iron-silica catalyst and found a

higher decomposition efficiency of phenol. Parida and Pradhan [22] prepared a series of Fe/meso-Al$_2$O$_3$ catalysts to investigate their degradation performance. They all confirmed that introducing aluminum could improve the efficiency of heterogeneous Fenton reaction. However, the exact role of Al in the catalytic process still demands further investigation.

The bimetallic oxide Fenton catalysts have been discussed by some researchers [23–25], but few of them have reported the bimetallic aluminum-silica catalyst. In this paper, a new efficient heterogeneous Fenton catalyst, Fe-Cu bimetallic supported aluminum-containing MCM-41, was fabricated by a co-precipitation method. Incorporating copper and aluminum with Fe significantly promoted phenol mineralization in the Fenton reaction at a wider pH range. According to the physicochemical characterization and catalytic performance analysis, the beneficial role of aluminum has been discussed.

2. Experimental

2.1. Materials

Ferric nitrate (Fe(NO$_3$)$_3$·9H$_2$O), copper nitrate (Cu(NO$_3$)$_2$·3H$_2$O) and aluminum sulfate (Al$_2$(SO$_4$)$_3$) were procured from Sinopharm Chemical Reagent Co., Ltd. Tetraethyl orthosilicate (TEOS) and cetyltrimethyl ammonium bromide (CTAB) were procured from Changshu Yanghu Chemical Co., Ltd. H$_2$O$_2$ and ammonia were obtained from Pinghu Chemical Reagent Factory. Phenol was supplied by Sangon Biotech (Shanghai) Co., Ltd. All chemicals were of analytical grade and without further purification.

2.2. Catalyst synthesis

In a typical sol–gel synthesis procedure, Fe(NO$_3$)$_3$·9H$_2$O and Cu(NO$_3$)$_2$·3H$_2$O were used as metallic sources. Specifically, 0.9 g of CTAB was dissolved in 60 mL of absolute ethanol and the mixed solution was stirred for 30 min. 0.1191 g of Fe(NO$_3$)$_3$·9H$_2$O and 0.0712 g of Cu(NO$_3$)$_2$·3H$_2$O were added in the CTAB solution and stirred for another 30 min to form solution A. In the meantime, 0.098 g of Al$_2$(SO$_4$)$_3$ was dissolved in 80 mL of deionized water, followed by adding 2 mL of TEOS and stirred for 1 h to form solution B. Then, solutions A and B were mixed together. After stirring for 1 h, 3.4 mL ammonia (25 wt%) was added to the mixed system dropwise to form a sol. The synthesis medium was kept under vigorous stirring condition for 6 h followed by aging for 12 h. The whole procedure was conducted at room temperature. The products were filtered, washed and dried at 110 °C. Finally, the crystallization and template removal were carried out in a muffle furnace at a rate of 1 K/min to 823 K, holding for 6 h. The calcined samples were designated as M4. Iron-containing MCM-41 material, which was designated as M2, was prepared following the same synthesis route except adding Cu(NO$_3$)$_2$·3H$_2$O in the solution A and Al$_2$(SO$_4$)$_3$ in the solution B, respectively. The bimetallic MCM-41 material was obtained without adding Al$_2$(SO$_4$)$_3$ in the solution B, and it was designated as M3. For blank reactions, pure silica MCM-41 material (designated as M1) was synthesized following a similar synthesis route. Finally, a washing process was done by immersing 1 g of calcined samples in a 1 L of dilute HNO$_3$ solution (pH 3) for 6 h to remove the loosely attached particles. The washed samples were filtered, dried, and calcined at 500 °C for 2 h.

2.3. Characterization of the samples

The physical or physiochemical properties of washed samples were characterized. The crystalline form of the samples was identified by a Rigaku D/max-2200/PC XRD instrument (Cu Kα radiation),

operating at 40 kV and 30 mA. The mesoporous phases of the samples were identified at the range of 0.5–8° with the scanning speed of 0.5°/min. Large diffraction angle analysis was conducted at the range of 10–70° by the same XRD instrument. The BET surface areas and pore size distribution of the samples were measured using a Micromeritics ASAP 2010 system with nitrogen as the adsorption gas. The compositional analysis of catalysts was performed after previously dissolution in HF acid by a high-resolution magnetic sector ICP-MS spectrometer (Iris Advantage 1000). To obtain the morphology of the sample, a high resolution-transmission electron microscopy (HRTEM, JEM100-CX, JEOL) was applied. The surface charges of all the samples were measured by Particle Size and Zeta Potential Analyzer (ZS90, Malvern Instruments Ltd., UK) based on electrophoretic mobility of the nanoparticles in aqueous media at different pH values. Each measurement was performed in an aqueous solution with a constant ionic strength (0.01 M KNO$_3$), and pH was adjusted by adding drops of NaOH or HNO$_3$ solution. X-ray photoelectron spectroscopy (XPS) measurements were carried out on a RBD upgraded PHI-5000C ESCA system (PerkinElmer Co., USA).
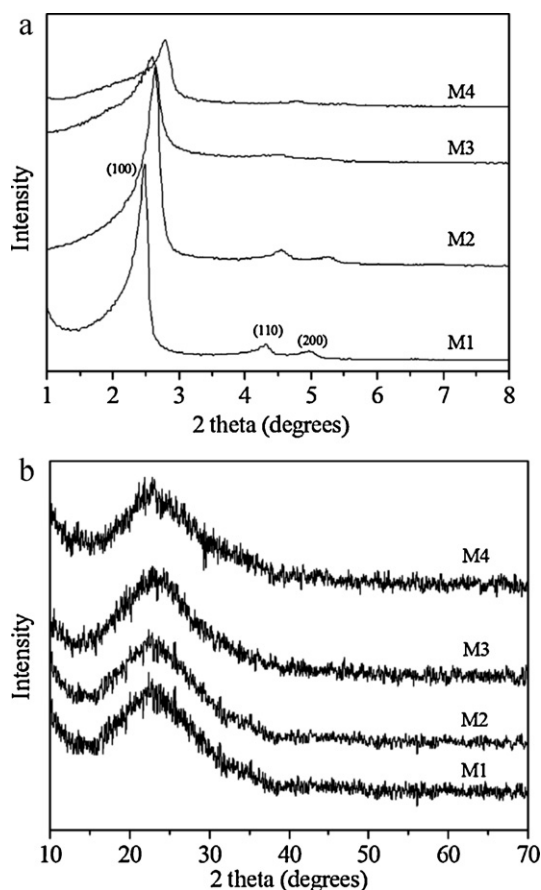
2.4. Catalytic performance

A series of batch experiments were carried out to measure the catalytic activity of the samples by degrading phenol in aqueous solutions. In a typical experiment, 0.03 g of catalyst was added into 20 mL of phenol solution in a flask (50 mL). The pH of the reaction medium was buffered by an appropriate amount of phosphate (0.05 M) to a given value. The covered flasks were kept at a mild temperature (40 °C) in a thermostatic oscillatory water bath. The suspension containing the catalyst and phenol was shaken in the dark for 20 min to achieve adsorption equilibrium. Then, a certain amount of H$_2$O$_2$ (30 wt%) was added to the suspension and initiated the degradation reaction. Each flask was taken out from the water bath at different time intervals and the supernatant solution was collected by filtration for TOC analysis using a TOC/TN analyzer (multi N/C 3000, Analytik Jena AG, Germany). The used catalyst was collected and regenerated by calcination at 500 °C for stability tests. Iron and copper contents in the filtered solutions after reaction were detected by atomic absorption spectrum (novAA 350, Germany). Analyses of intermediate products were performed by high performance liquid chromatography (HPLC-2010A, Shimadzu) with a SHIM PACK C18 chromatographic column (250 mm). The determination of H$_2$O$_2$ concentration in reaction solution was conducted following Nogueira's method [26].

3. Results and discussion

3.1. Physicochemical characterizations

The X-ray diffraction spectra of the washed mesoporous samples (M1, M2, M3 and M4) are shown in Fig. 1. In the small angle range (Fig. 1a), the XRD pattern of pure MCM-41 (M1) exposes a typical mesoporous structure with three well-resolved peaks which are indexed as (1 0 0), (1 1 0) and (2 0 0) diffractions. With the incorporation of metal species, the (1 0 0) peak of each sample was preserved. This indicates that the doped samples still have MCM-41 mesoporous structures. It should be noticed that the peak intensities of the modified samples decrease gradually with the increase in metal incorporation, suggesting that a less ordered structure was formed. Additionally, the (1 0 0) peaks for the doped samples shifted slightly to higher 2θ values, indicating that after incorporation the pore size got slightly smaller [27], as presented in Table 1. In the large angle XRD patterns (Fig. 1b), the broad peak at about 23° refers to amorphous silica. Besides, no other peaks can be found in the large angle XRD diffraction patterns. Due to low metal

Fig. 1. (a) Small angle XRD patterns of synthesized samples; (b) large angle XRD patterns of synthesized samples.

regularization of mesoporous structures. The deteriorated pore structure is probably attributed to the unfavorable effects of high content metal oxides on the ordered MCM-41 structure. However, the addition of Al could stabilize the MCM-41 framework by forming aluminosilicate to minimize the negative influence of other metals on the ordered structure [28].

Nitrogen adsorption isotherms and BJH pore size distributions of the samples are illustrated in Figs. 3 and 4, respectively. All samples exhibit type IV N_2 adsorption isotherms, corresponding to their uniform hexagonal mesoporous structure with a narrower pore size distribution [29]. The inflections at $p/p_0 = 0.2$–0.3 in the isotherms become sharper with the reduced level of metal incorporation, which suggests the increasing order of mesoporous structures. This is consistent with the XRD results. In addition, both the isotherms of M3 and M4 show a small hysteresis loop at higher relative pressure ($p/p_0 > 0.8$). The observed loop may reflect the macro pores of interparticles [30,31]. As a result, the BJH average pore sizes of M3 and M4 (3.88 nm) are much larger than that for M1 and M2 (2.91 nm). The unit cell parameter (a_0), calculated from $2d_{100}/\sqrt{3}$, together with other structural and chemical properties of the washed samples, is presented in Table 1. With the increase in metals, BET surface areas of the samples decreased from 1545.60 to 1062.55 m^2/g. An inverse trend is observed in the case of pore volume. This may be attributed to the decrease in wall thickness and the presence of macro pores.

The amount of acidic oxygen-containing surface groups existing in the samples can be estimated by measuring their zeta potentials. From Fig. 5, the point of zero charge (PZC) of M1 is at pH 2.25. With the lifting level of metal incorporation, the PZC shifted to lower pH values. According to Tamura et al. [32], metal oxides in aqueous solution can form surface hydroxyl groups by dissociative chemisorption of water molecules. The addition of metals in mesoporous silica increased the concentration of the surface unsaturated metal centers. As a result, with the increase in the surface acidic groups, the surface acidity of the modified samples was enhanced. The FTIR results can further support this conclusion. As seen in Fig. 6 (region 1), a strong sharp absorption bands appeared at 3400–3500 cm^{-1} associated with the surface hydroxyl groups [33]. The increasing intensity of such band indicates that more and more surface acidic groups were formed. The increase in surface oxygen-containing groups causes the samples to be more negative charged and to exhibit the decreased PZC value [34].

3.2. Preliminary experiments

3.2.1. Comparison experiments

In a preliminary study, a batch of experiments was executed under a given condition (pH 4, catalyst dosage = 1.5 g/L, temperature = 40 °C, initial concentration = 200 mg/L and H_2O_2 dosage = 0.049 mol/L) to evaluate the catalytic activities of samples. The control experiments using M1 with and without adding H_2O_2 were also conducted. Fig. 7 shows the evolution of TOC abatement within the reaction time for these experiments. Using M1 as the catalyst only got 5% of TOC reduction after 2 h reaction, which might

loading level in our study, the deposited metals were highly dispersed as very small metal oxides particles. TEM results provided further support: no cognizable metal oxides aggregation was seen in Fig. 2.

The TEM images of the samples are shown in Fig. 2. It is confirmed that all the samples are characterized as the mesoporous materials with well-ordered two-dimensional hexagonal mesostructure. Obviously, introducing metal species in the synthesis media did not affect the framework of the mesoporous materials. The metal particles are well dispersed throughout the silica framework. This result is highly consistent with the analysis of XRD and N_2 adsorption/desorption isotherms. The sample M1 is standard spherical with particles 200–300 nm in diameter (Fig. 2a). Other samples have almost the same dimensions as M1 but their morphologies become slightly irregular. From Fig. 2, it can be seen that the mesoporous structure of M3 is worst (image c), and M4 owns a better structure (image d). It seems that the addition of Cu would deteriorate the pore structure but Al could improve the

Table 1
The structural and chemical properties of synthesized samples.

Sample	S_{BET} (m^2/g)	V_p (cm^3/g)[a]	d_{100} (Å)	a_0 (Å)	p_d (Å)[b]	w_d (Å)[c]	d_p (nm)[d]
M1	1545.60	0.83	35.70	41.22	20.45	20.77	2.63
M2	1402.53	0.86	33.52	38.71	23.23	15.48	2.67
M3	1165.52	1.11	33.99	39.24	23.93	15.31	3.91
M4	1062.55	0.93	34.68	40.05	25.90	14.15	3.95

[a] Total pore volume.
[b] Pore diameter (D_{BJH}).
[c] Wall thickness = unit cell parameter (a_0) – pore size (p_d).
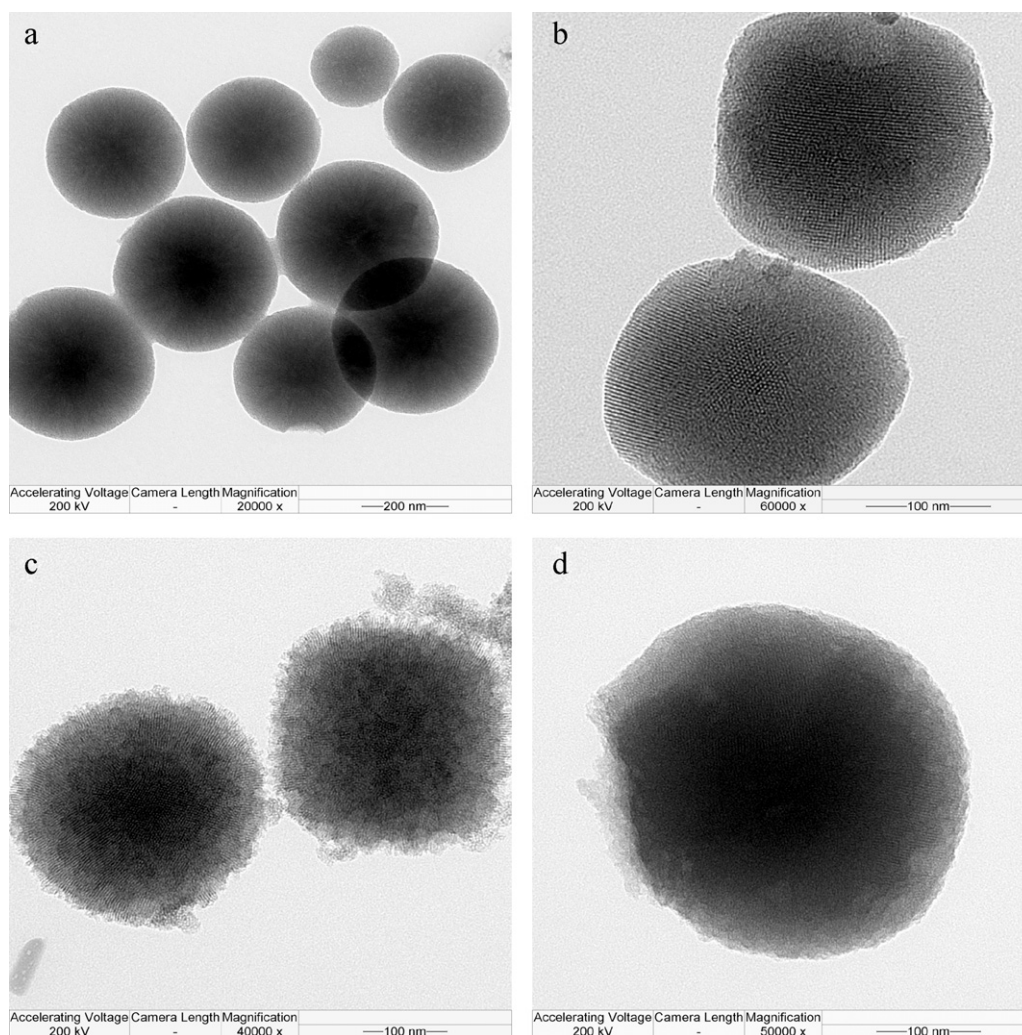[d] Average pore diameter, calculated by BJH method.

Fig. 2. TEM micrographs of synthesized samples: (a) M1; (b) M2; (c) M3; (d) M4.

attribute to the adsorption by M1 and oxidation by H_2O_2 (curve b). However, M2 could achieve 12% of TOC abatement after 2 h of reaction (curve d). With the addition of Cu, M3 raised this value to 35% (curve e), which clearly evidenced the role of copper in Fenton reaction at pH > 4 [23]. Apparently, the more the metals introduced, the higher the activity owned by the catalyst. It is noteworthy that,

compared to M3, M4 has comparable content of iron and copper, and a declined surface area, as presented in Tables 1 and 2. However, M4 shows an optimal efficiency that achieved an abatement value of ca. 48% in 2 h (curve f). The introduced aluminum contributed to the relevant enhancement of TOC reduction. In addition to favoring the well dispersion of active sites [20], aluminum could also play a crucial role in the Fenton reaction.
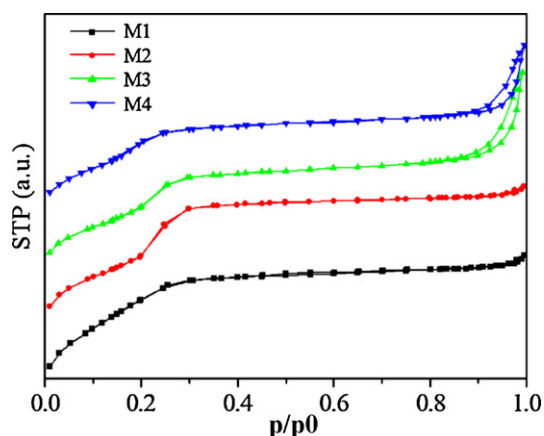

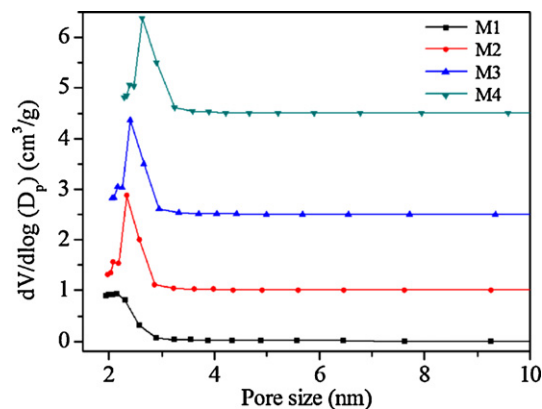**Fig. 3.** Nitrogen adsorption isotherms of M1, M2, M3 and M4.

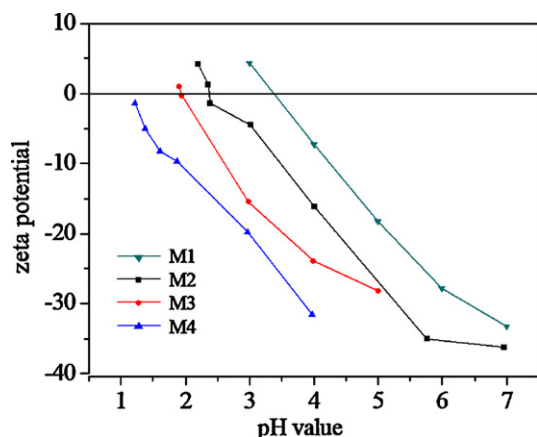**Fig. 4.** BJH pore size distributions of M1, M2, M3 and M4.

Fig. 5. Zeta potential measurements of M1, M2, M3 and M4 as a function of pH.
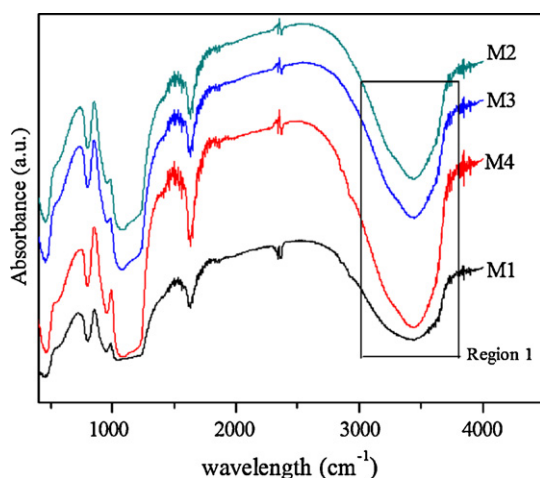

Fig. 6. FTIR spectra of M1, M2, M3 and M4.

3.2.2. Stability test of the samples

The iron and copper concentrations in the reaction solution of M3 and M4 during 2 h were tracked to assess the stability of catalysts. The obtained results presented a rising tendency throughout
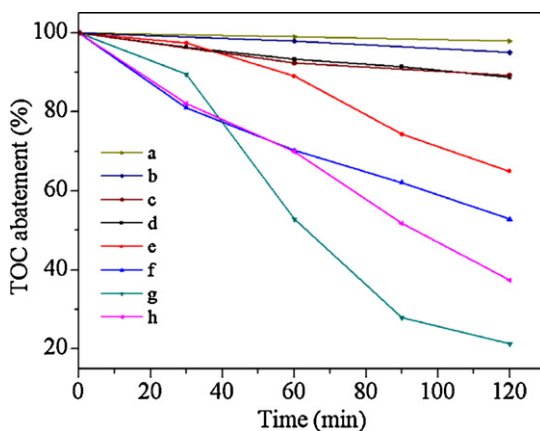
Table 2
Metal compositions in synthesized samples.

Sample	Incorporated metal after washing (wt%)		
	Fe	Cu	Al
M2	2.55	–	–
M3	3.37	2.18	–
M4	2.98	2.09	1.43

the whole reaction. At the end of reaction, 2.60 mg/L of Fe(III) and 7.76 mg/L of Cu(II) were found in the M4 solution while 4.89 mg/L of Fe(III) and 10.60 mg/L of Cu(II) in the M3 solution. The presence of Al appears to improve the stability of active sites in the catalyst. To investigate the effect of dissolved metal ions on degradation, a homogeneous experiment using M1 with 5.0 mg/L of Fe(III) and 8.0 mg/L of Cu(II) was conducted and got only 11% of the TOC abatement (curve c), indicating that the observed TOC removal was mainly attributed to heterogeneous catalytic reactions. Furthermore, to determine the effect of phosphate buffer, a control experiment (M4 as catalyst) without phosphate buffer was performed. Noticeably, at the end of 2 h reaction, the catalyst demonstrated a higher efficiency, corresponding to 79% of TOC abatement (curve g). In the meantime, the solution pH descended to 2.6 and 13.2 mg/L of Fe(III) and 16.6 mg/L of Cu(II) were detected in the solution. The contribution of the homogeneous Fenton reaction in such system has been evaluated by another control test: using M1 with 13.0 mg/L of Fe(III) and 16.0 mg/L of Cu(II) for phenol degradation under the same condition and getting 63% of the TOC abatement (curve h). Apparently, without buffer solution, the phenol degradation led to a decreased pH. However, in a more acidic solution, active metal sites in the catalyst became unstable and the homogeneous Fenton-like reactions tended to be dominant in the degradation process. Therefore, in our reaction system, to minimize the leaching of metal ions, keep the stability of catalyst and analyze the mechanism, it is important to maintain solution pH by using the phosphate buffer solution.

At the end of reaction, M4 was recovered from the reaction solution by filtration. After regeneration at 500 °C for 3 h, the catalyst was treated with the phenol solution under same condition for another two cycles to figure out the reusability of the catalyst. The leached metal ions were monitored when each cycle was finished. The obtained data demonstrated an enhancing stability for the reused catalysts, being more accentuated for copper species (7.76 mg/L in the 1st run, 1.31 mg/L in the 2nd run and 0.34 mg/L in the 3rd run) [24]. The catalytic behavior of M4 was reproducible (Fig. 8) in the consecutive experiments without a
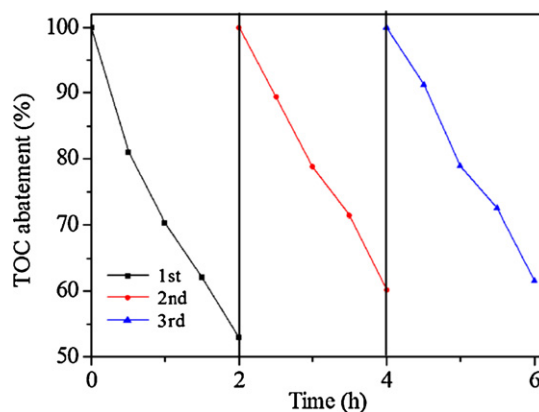

Fig. 7. Comparison of phenol degradation: (a) M1 without H_2O_2; (b) M1 with H_2O_2; (c) 5.0 mg/L of Fe^{3+} ions and 8 mg/L of Cu^{2+} ions; (d) M2 with H_2O_2; (e) M3 with H_2O_2; (f) M4 with H_2O_2; (g) M4 with H_2O_2 in the non-buffered solution; (h) M1 with 13.0 mg/L of Fe^{3+} and 16.0 mg/L of Cu^{2+} in the non-buffered solution. Reaction conditions: pH 4, catalyst dosage = 1.5 g/L, temperature = 40 °C, initial phenol concentration = 200 mg/L and H_2O_2 dosage = 0.049 mol/L.

Fig. 8. Reusability of M4 after subsequent reactions. Reaction conditions: pH 4, catalyst dosage = 1.5 g/L, temperature = 40 °C, initial phenol concentration = 200 mg/L and H_2O_2 dosage = 0.049 mol/L.

remarkable drop in the efficiency. The observed decrease in efficiency can be attributed to the leaching of active sites and the decline in contribution of homogeneous Fenton reaction.

3.2.3. The evolution of intermediates in degradation

The intermediate products formed during degradation were identified by HPLC analysis (M4 as catalyst). After 30 min reaction, catechol and hydroquinone appeared as the major by-products and phenol was still detectable in the solution. The formation of catechol and hydroquinone could be attributed to $HO^\bullet$ attack on the 2 and 4 positions versus the —OH group in the aromatic ring. As the catalytic degradation went on, phenol and catechol disappeared in the solution. However, hydroquinone concentration reduced gradually due to its much lower decomposition rate [35]. In addition, carboxylic acid intermediaries such as oxalic acid, formic acid and acetic acid were perceived in the reaction mixture which indicated the opening of the aromatic cycle. Basing on the obtained results, it could be rationalized considering that the remaining TOC was mainly composed of carboxylic acids and hydroquinone.

3.3. Effect of parameters on Fenton oxidation of phenol solution

In this section, the regenerated M3 and M4 catalysts (denoted as M3-3rd and M4-3rd), which had been used twice, were employed for the following tests due to their negligible homogeneous contribution to the whole degradation (as mentioned in Section 3.2.2).

3.3.1. Effect of temperature

In order to verify the effect of temperature on the oxidation of phenol solution, a series of experiments were carried out at three different temperatures (pH 4, catalyst dosage = 1.5 g/L, initial concentration = 200 mg/L and H_2O_2 dosage = 0.049 mol/L). The results are shown in Fig. 9a. Obviously, an increase in temperature has a positive impact on the mineralization of phenol solution. The TOC removal increases from 11% to 47% as the temperature is elevated from 25 to 60 °C. Higher temperature appears to accelerate the decomposition of H_2O_2 into hydroxyl radicals, and therefore improves degradation. However, ascending temperature also accelerates the thermal decomposition of H_2O_2 into oxygen and water, and consequently aggravates H_2O_2 consumption and decreases the utilization efficiency of H_2O_2 [36,37]. Therefore, it is important to choose an appropriate reaction temperature.

3.3.2. Effect of pH

The pH value is one of the decisive factors in the Fenton process. It affects the activity of the oxidant and the substrate, the speciation of iron, and the decomposition of hydrogen peroxide [38]. In this paper, phenol solution was adjusted to three different pH values to check the role of pH in the catalytic reaction and evaluate the performance of M4 in a wide pH range (catalyst dosage = 1.5 g/L, temperature = 60 °C, initial phenol concentration = 200 mg/L and H_2O_2 dosage = 0.049 mol/L). All chosen pH points were equal to or greater than 4 to avoid notable iron or copper leaching into the reaction solution. Therefore, the homogeneous contribution of the leached metals could be ignored. Fig. 9b presents the degradation efficiency with different reaction pH values and as a function of time. A decrease in TOC abatement is observed at higher pH values. This can be attributed to the fact that at higher pH, H_2O_2 would rapidly decompose into molecular oxygen and H_2O but not transform into hydroxyl radicals, accordingly with oxidizing ability loss [39]. Additionally, it should be noticed that at pH 5 and 7, the reused M4 still yielded a certain amount of catalytic activity. The doped Cu would be one reason for such observation. As claimed by Lam and Hu [23], at pH > 4, copper could play a dominant role in bimetallic catalyst for Fenton type reaction, and iron would further promote the catalytic performance at a relatively wide pH range. Anyway,
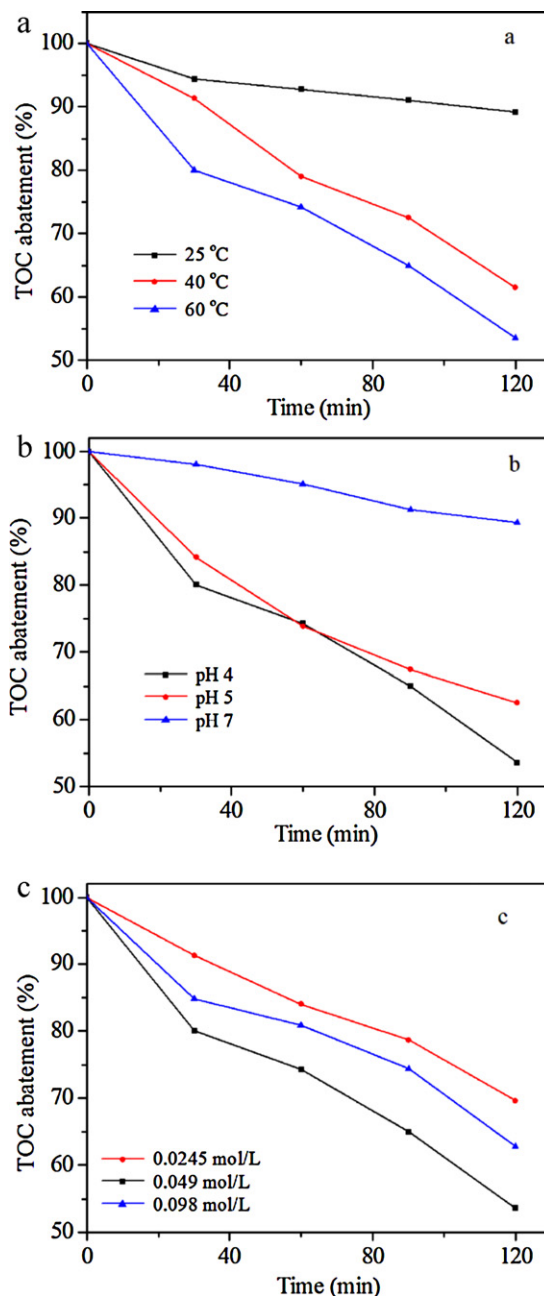

Fig. 9. Effect of experimental parameters on phenol degradation: (a) effect of temperature; (b) effect of pH values; (c) effect of H_2O_2 dosage. Except for the investigated parameters other parameters fixed on pH 4, catalyst dosage = 1.5 g/L, temperature = 60 °C, initial phenol concentration = 200 mg/L and H_2O_2 dosage = 0.049 mol/L.

it is a big challenge to achieve desirable reaction rate at circum-neutral pH in practical application of wastewater treatment due to the consideration of cost and convenience. Further efforts should be made on this.

3.3.3. Effect of H_2O_2 dosage

The effect of H_2O_2 dosage on phenol degradation was investigated by varying H_2O_2 dosage (0.0245, 0.049 and 0.098 mol/L) under a given reaction condition (pH 4, catalyst dosage = 1.5 g/L, temperature = 60 °C and initial concentration = 200 mg/L) and the results are shown in Fig. 9c. When H_2O_2 dosage increased from 0.0245 to 0.049 mol/L, the TOC removal percentages increased correspondingly from 31% to 47%. The increase in H_2O_2 concentration
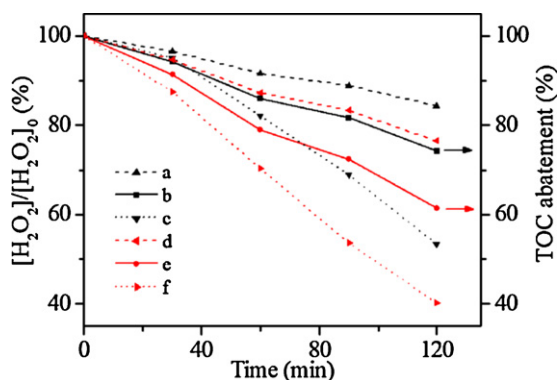
Fig. 10. H_2O_2 and TOC reduction tendency for M3-3rd (black line) and M4-3rd (red line): (a) and (d) theoretical value of H_2O_2 decomposition for phenol mineralization; (b) and (e) TOC abatement; (c) and (f) practical consumption of H_2O_2. Reaction conditions: pH 4, catalyst dosage = 1.5 g/L, temperature = 40 °C, initial phenol concentration = 200 mg/L and H_2O_2 dosage = 0.049 mol/L. (For interpretation of the references to color in this figure legend, the reader is referred to the web version of the article.)

in the solution leads to an increase in the formation of HO• [40]. However, when given higher H_2O_2 dosage, the TOC removal was not further enhanced but dropped down. This is because at high H_2O_2 concentration there is a competition of HO• consumption between the substrate and H_2O_2. As expressed in Eqs. (3) and (4), H_2O_2 in high concentration acts as a scavenger of the highly potent HO•, and HO• would recombine to form H_2O and O_2 [41]. Therefore, it is necessary to select an optimal H_2O_2 dosage for the heterogeneous Fenton reaction.

$$H_2O_2 + OH^\bullet \rightarrow H_2O + HOO^\bullet \tag{3}$$

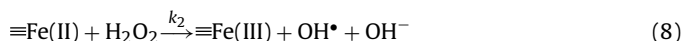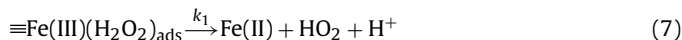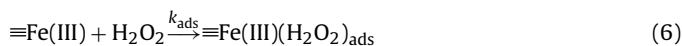$$HOO^\bullet + OH^\bullet \rightarrow H_2O + O_2 \tag{4}$$

3.4. Decomposition of H_2O_2

In addition to TOC removal, the reduction tendency of H_2O_2 was discussed using M3-3rd and M4-3rd as catalyst, respectively. Like the evolution of TOC, the concentration of H_2O_2 in two solutions decreased as the reaction proceeded (Fig. 10). However, H_2O_2 decayed much greater than theoretical value calculated by Eq. (5) [42]. It could be understood that: (1) a portion of H_2O_2 was decomposed to H_2O and O_2 which had no contribution to TOC removal; (2) as radical scavenger, phosphate buffer would lower the HO• concentration in the solution. Furthermore, the decomposition of H_2O_2 was faster in the M4 system than that in the M3 system. The observed enhancement was mainly due to the addition of Al. After 2 h reaction, in the M3 system, about 47% of H_2O_2 was reduced corresponding to 26% of TOC removal, in which theoretical H_2O_2 usage is about 16% and the apparent utilization ratio of H_2O_2 is only 34%. On the other side, in the M4 system, 60% of H_2O_2 was reduced corresponding to 39% of TOC removal, corresponding to a utilization ratio of H_2O_2 of 42%. Apparently, the utilization ratio of H_2O_2 was enhanced in the M4 system, which suggested that in the M4 system a higher proportion of H_2O_2 was decomposed into HO•, and the decomposition of H_2O_2 into H_2O and O_2 has been suppressed.

$$C_6H_6O + 14H_2O_2 \rightarrow 17H_2O + 6CO_2 \tag{5}$$

3.5. Mechanism discussion

Once incorporating both iron and copper into the aluminum-containing MCM-41, the catalyst showed an enhanced activity in the phenol mineralization under mild conditions. According to the Haber–Weiss mechanism [43,44], Fe(III) initiated H_2O_2

decomposition starts from the reduction of Fe(III) and the formation of HO$_2^\bullet$ ($O_2^{\bullet-}$), followed by the generation of hydroxyl radicals and the transformation of reduced Fe species. The initial step is regarded as the rate determining step. However, at pH ≥ 4 in a heterogeneous system, the catalytic reaction mainly occurs on the catalyst surface. The anchoring of H_2O_2 to active metal centers should be achieved before the Fe(III) initiated H_2O_2 decomposition process (Eq. (6)). The hydroxyl radical concentration is proportional to the concentration of $\equiv$Fe(III)(H_2O_2)$_{ads}$, which is determined from the kinetics of H_2O_2 adsorption (k_{ads}) [45]. Therefore, the adsorption of H_2O_2 onto the metal centers plays an important role in this heterogeneous Fenton reaction.

$$\equiv\text{Fe(III)} + H_2O_2 \xrightarrow{k_{ads}} \equiv\text{Fe(III)}(H_2O_2)_{ads} \tag{6}$$

$$\equiv\text{Fe(III)}(H_2O_2)_{ads} \xrightarrow{k_1} \equiv\text{Fe(II)} + HO_2 + H^+ \tag{7}$$

$$\equiv\text{Fe(II)} + H_2O_2 \xrightarrow{k_2} \equiv\text{Fe(III)} + OH^\bullet + OH^- \tag{8}$$

To evaluate the surface properties of the catalysts after Al incorporation, the XPS spectra of M3 and M4 have been measured (Fig. 11). Concretely, Cu $2p_{3/2}$ and Cu $2p_{1/2}$ peaks locating at 934.7 and 954.9 eV in the spectrum of M3 shift to 934.1 and 954 eV in M4, respectively. Meanwhile, Fe $2p_{3/2}$ at 713.6 eV in M3 shifts to 712.5 eV in M4. Such downward shift of both metals in the XPS spectra is a piece of evidence to demonstrate the change in their electronic density. It is most likely that the doped Al could act as an electron donor to increase the electron density of the active metal centers. It can be understood from their electronegativities that
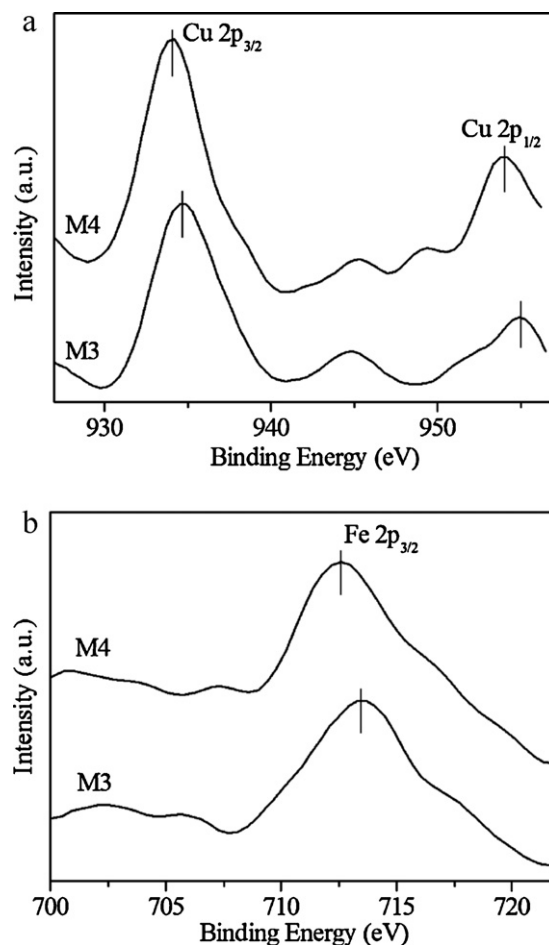
Fig. 11. XPS spectra for M3 and M4: (a) Cu 2p; (b) Fe 2p.
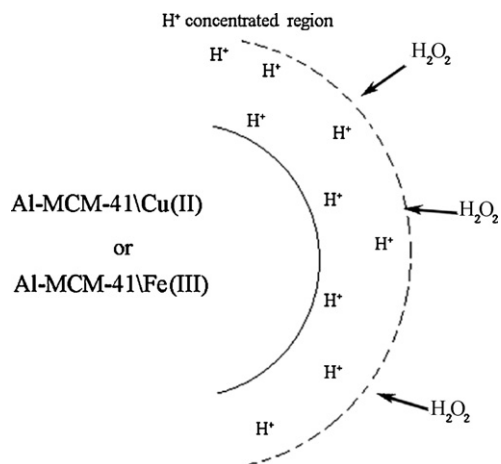
Scheme 1. H$^+$-concentrated region on the surface of catalyst.

both Fe and Cu are larger than Al. Therefore, in a bonding situation close to Al, Fe(Cu) centers possess improved electron densities. As an electrophilic reagent, H$_2$O$_2$ is more prone to combine with the metal centers with higher electron density. The enhanced H$_2$O$_2$ adsorption could promote Eqs. (7) and (8) and the whole Fenton catalytic reaction would be accelerated.

Moreover, according to the observed zeta potential results (Fig. 5), the introduction of aluminum resulted in an increase in acidic oxygen-containing surface groups. These functional groups themselves and the aluminum centers do not promote the OH$^\bullet$ generation [46]. However, the more negative surface charges over the catalysts enable the formation of an H$^+$-concentrated region close to the catalyst surface (Scheme 1) [47]. Compared to the bulk aqueous solution, the protons (H$^+$) over the catalyst surface appear to be in higher concentration; therefore, in the microscopic localized ambience, the decomposition of adsorbed H$_2$O$_2$ into H$_2$O and O$_2$ has been greatly suppressed [48]. Consequently, more H$_2$O$_2$ would react with active sites via Fenton process and result in a higher OH$^\bullet$ generation. The synergic effect of surface acidic groups and the higher electron density of active metal centers result in the improved catalytic activity of this new heterogeneous Fenton catalyst.

4. Conclusion

A Fe–Cu bimetal-based aluminum-containing MCM-41 Fenton catalyst was successfully synthesized via a co-precipitation method under ambient conditions. The catalyst held a typical mesoporous structure with regular hexagonal pore arrangements as illustrated by XRD, nitrogen physisorption and TEM analyses. The elevated catalytic activity and stability for phenol degradation were observed. Such experimental conditions as pH value, H$_2$O$_2$ dosages and reaction temperature have been investigated. It was found that higher temperature had a positive effect on mineralization; excess H$_2$O$_2$ would act as a scavenger of HO$^\bullet$; copper could make the catalyst less pH dependent and keep activity even at circumneutral pH. With further support of XPS, zeta potential and the analyses of H$_2$O$_2$ utilization ratio, the reasons for the beneficial role of Al have been proposed. With the incorporation of aluminum, the improved electron density of active metal centers favored the adsorption of H$_2$O$_2$, and the H$^+$ concentrated region over the catalyst surface favored the conversion of H$_2$O$_2$ into highly active species but not decomposition into H$_2$O and oxygen. The catalyst was proved to be applied as an attractive alternative in the heterogeneous Fenton catalysis, and

the implication of Al revealed new strategies in the development of novel effective Fenton catalysts.

References

[1] E. Brillas, E. Mur, R. Sauleda, L. Sànchez, J. Peral, X. Domènech, J. Casado, Appl. Catal. B: Environ. 16 (1998) 31–42.
[2] P. Bautista, A.F. Mohedan, J.A. Casas, J.A. Zazo, J.J. Rodriguez, J. Chem. Technol. Biotechnol. 83 (2008) 1323–1338.
[3] M. Pera-Titus, V. García-Molina, M.A. Baños, J. Giménez, S. Esplugas, Appl. Catal. B: Environ. 47 (2004) 219–256.
[4] P. Maletzky, R. Bauer, J. Lalmsteiner, B. Pouresmael, Chemosphere 38 (1999) 2315–2325.
[5] S. Caudo, C. Genovese, S. Perathoner, G. Centi, Microporous Mesoporous Mater. 107 (2008) 46–57.
[6] J.Y. Feng, X.J. Hu, P. Yue, Environ. Sci. Technol. 38 (2004) 269–275.
[7] G. Centi, S. Perathoner, T. Torre, M.G. Verduna, Catal. Today 55 (2000) 61–69.
[8] N.H. Phu, T.T.K. Hoa, N.V. Tan, H.V. Thang, P.L. Ha, Appl. Catal. B: Environ. 34 (2001) 267–275.
[9] D.J. Doocey, P.N. Sharratt, Saf. Environ. 82 (2004) 352–358.
[10] M. Tekbaş, H.C. Yatmaz, N. Bektaş, Microporous Mesoporous Mater. 115 (2008) 594–602.
[11] L.G. Devi, S.G. Kumar, K.M. Reddy, C. Munikrishnappa, J. Hazard. Mater. 164 (2009) 459–467.
[12] A.R. Khataee, V. Vatanpour, A.R.A. Ghadim, J. Hazard. Mater. 161 (2009) 1225–1233.
[13] Z. Eren, N.H. Ince, J. Hazard. Mater. 177 (2010) 1019–1024.
[14] Y. Yang, P. Wang, S. Shi, Y. Liu, J. Hazard. Mater. 168 (2009) 238–245.
[15] M. Masarwa, H. Cohen, D. Meyerstein, D.L. Hickman, A. Bakac, J.H. Espenson, J. Am. Chem. Soc. 110 (1988) 4293–4297.
[16] A.C.K. Yip, F.L.Y. Lam, X.J. Hu, Chem. Eng. Sci. 62 (2007) 5150–5153.
[17] I.R. Guimaraes, A. Giroto, L.C.A. Oliveira, M.C. Guerreiro, D.Q. Lima, J.D. Fabris, Appl. Catal. B: Environ. 91 (2009) 581–586.
[18] B.B. Fan, H.Y. Li, W.B. Fan, C. Jin, R.F. Li, Appl. Catal. A: Gen. 340 (2008) 67–75.
[19] Y.L. Nie, C. Hu, J.H. Qu, X. Zhao, Appl. Catal. B: Environ. 87 (2009) 30–36.
[20] H. Lim, J. Lee, S. Jin, J. Kim, J. Yoon, T. Hyeon, Chem. Commun. 46 (2006) 3–465.
[21] A.L. Pham, C. Lee, F.M. Doyle, D.L. Sedlak, Environ. Sci. Technol. 43 (2009) 8930–8935.
[22] K.M. Parida, A.C. Pradhan, Ind. Eng. Chem. Res. 49 (2010) 8310–8318.
[23] F.L.Y. Lam, X. Hu, Catal. Commun. 8 (2007) 2125–2129.
[24] J.A. Melero, G. Calleja, F. Martínez, R. Molina, Catal. Commun. 7 (2006) 478–483.
[25] S. Navalon, R. Martin, M. Alvaro, H. Garcia, Angew. Chem. Int. Ed. 49 (2010) 8403–8407.
[26] R.F.P. Nogueira, M.C. Oliveira, W.C. Paterlini, Talanta 66 (2005) 86–91.
[27] K.M. Parida, D. Rath, J. Colloid Interface Sci. 340 (2009) 209–217.
[28] R. Nares, Jorge Ramírez, A. Gutiérrez-Alejandre, R. Cuevas, Ind. Eng. Chem. Res. 48 (2009) 1154–1162.
[29] S.C. Laha, R. Kumar, Microporous Mesoporous Mater. 53 (2002) 163–177.
[30] K.S.W. Sing, D.H. Everett, R.A.W. Haul, L. Moscou, R.A. Pierotti, J. Rouquerol, T. Siemieniewska, Pure Appl. Chem. 57 (1985) 603–619.
[31] K.P. Kumar, J. Kumar, J. Keizer, J. Am. Chem. Soc. 77 (1994) 1396–1400.
[32] H. Tamura, K. Mita, A. Tanaka, M. Ito, J. Colloid Interface Sci. 243 (2001) 202–207.
[33] D. Rath, K.M. Parida, Ind. Eng. Chem. Res. 50 (2011) 2839–2849.
[34] C. Moreno-Castilla, M.A. Ferro-García, J.P. Joly, I. Bautista-Toledo, F. Carrasco-Marín, J. Rivera-Utrilla, Langmuir 11 (1996) 4386–4392.
[35] R. Niessen, D. Lenoir, P. Boule, Chemosphere 17 (1988) 1977–1984.
[36] A.M.F.M. Guedes, L.M.P. Madeira, R.A.R. Boaventura, C.A.V. Costa, Water Res. 37 (2003) 3061–3069.
[37] J.H. Ramirez, C.A. Costa, L.M. Madeira, Catal. Today 107–108 (2005) 68–76.
[38] H. Zhang, H.J. Choi, C.P. Huang, J. Hazard. Mater. B125 (2005) 166–174.
[39] J. Guo, M. Al-Dahhan, Ind. Eng. Chem. Res. 42 (2003) 2450–2460.
[40] R. Idel-aouad, M. Valiente, A. Yaacoubi, B. Tanouti, M. López-Mesas, J. Hazard. Mater. 188 (2011) 745–750.
[41] K. Dutta, S. Mukhopadhyay, S. Bhattacharjee, B. Chaudhuri, J. Hazard. Mater. B84 (2001) 57–71.
[42] S. Navalon, M. Alvaro, H. Garcia, Appl. Catal. B: Environ. 99 (2010) 1–26.
[43] S.S. Lin, M.D. Gurol, Environ. Sci. Technol. 32 (1998) 1417–1423.
[44] W.P. Kwan, B.M. Voelker, Environ. Sci. Technol. 37 (2003) 1150–1158.
[45] F. Haber, J. Weiss, Proc. R. Soc. Lond. A 147 (1934) 332–351.
[46] J.A. Zazo, A.F. Fraile, A. Rey, A. Bahamonde, J.A. Casas, J.J. Rodriguez, Catal. Today 143 (2009) 341–346.
[47] J.S. Lee, W.Y. Choi, Environ. Sci. Technol. 39 (2005) 6800–6807.
[48] L.B. Khalil, B.S. Girgis, T.A. Tawfik, J. Chem. Technol. Biotechnol. 76 (2001) 1132–1140.